Optogenetic protein clustering and signaling activation in mammalian cells

Lukasz J Bugaj[1,2], Atri T Choksi[1], Colin K Mesuda[3], Ravi S Kane[4,5] & David V Schaffer[1–3,6,7]

We report an optogenetic method based on *Arabidopsis thaliana* cryptochrome 2 for rapid and reversible protein oligomerization in response to blue light. We demonstrated its utility by photoactivating the β-catenin pathway, achieving a transcriptional response higher than that obtained with the natural ligand Wnt3a. We also demonstrated the modularity of this approach by photoactivating RhoA with high spatiotemporal resolution, thereby suggesting a previously unknown mode of activation for this Rho GTPase.

Regulation of cellular function requires precise modulation of the intensity, location and duration of signaling events[1]. Protein oligomerization—the assembly of proteins into multimers—is a particularly powerful mechanism for modulating cellular signaling, and it is used to activate broad classes of proteins including membrane receptors, receptor ligands, kinases, transcription factors and numerous other cytosolic signaling effectors. Oligomerization enables ultrasensitive digital signaling responses, connects nanoscale protein activity to microscale control of cellular structures, provides scaffolds for assembly of enzymatic activities and participates in disease pathologies[2].

Studying the impact of protein oligomerization on cell behavior has been challenging because of the lack of approaches to exert tunable control over a protein's oligomeric state. Transmembrane receptors can be clustered using antibodies, and intracellular targets can be oligomerized with small molecule–dependent dimerization of repeated inducible dimerizing domains[3]. Owing to their reliance on biochemical agents to mediate clustering, however, these techniques suffer from limited spatial resolution and are incapable of dynamic protein regulation.

Optogenetic systems[4] have recently demonstrated precise and reversible control of signaling pathways through light-mediated protein heterodimerization[5–9] and homodimerization[10]. Though these are important modes for regulating protein activity, numerous signaling events require the assembly of proteins into higher-order oligomers. Here we present a genetically encoded platform for modular and tunable control of protein oligomerization, and we demonstrate its broad utility for controlling diverse intracellular signaling cascades.

A. thaliana cryptochrome 2 (Cry2, NCBI Reference Sequence NM_179257) forms oligomeric 'photobodies' in plant cells in response to blue light[11], but this property has not been reported in mammalian cells. Upon transfection into human embryonic kidney (HEK) 293T cells, the photolyase homology region (PHR) of Cry2 fused to mCherry (Cry2-mCh) formed distinct fluorescent puncta within 10 s of blue light illumination (**Fig. 1a**,**b** and **Supplementary Video 1**; full construct details in **Supplementary Table 1**). Upon withdrawal of blue light, the clusters dispersed to their original state within minutes (**Fig. 1b**). Notably, clustering was not observed with a light-insensitive Cry2 mutant harboring a D387A mutation[12] (**Fig. 1c**). From a diffuse initial condition, Cry2-mCh fluorescence could be repeatedly clustered and unclustered with similar kinetics (**Fig. 1d**,**e**). Three-dimensional reconstruction of single cells expressing clustered Cry2-mCh revealed heterogeneity in the size of such clusters (**Supplementary Video 2**), and fluorescence recovery after photobleaching (FRAP) analysis of individual clusters demonstrated rapid fluorescence recovery (**Supplementary Fig. 1**), suggesting that in the light state the oligomers dynamically exchange Cry2-mCh subunits with the bulk and/or one another (**Supplementary Fig. 2**).

Cry2 clustering was not reported in a recent study that focused on light-dependent Cry2-CIB1 interactions in mammalian cells[5]. In the presence of cytosolic CIB1, we found that Cry2 still clustered (**Supplementary Fig. 3**) and that CIB1 colocalized with these clusters, which indicates that CIB1 interaction does not preclude Cry2 clustering and may even offer a means to assemble two proteins into a cluster.

In parallel with an increase in oligomer size, the number of visible clusters in a cell increased sigmoidally over time upon illumination (**Fig. 1f**). Fitting this relationship to a sigmoidal function allowed us to extract $T_{1/2}$, the time at which a half-maximal number of visible clusters was detected. This metric of association kinetics was dependent on light intensity (Jonckheere-Terpstra trend analysis[13] (Online Methods), $P = 0.004$, $n = 4$, **Fig. 1g**). Upon light withdrawal, cluster number followed a single exponential decay with a time constant τ of ~5.5 min (**Fig. 1e**), consistent with a previous report of the lifetime of the activated Cry2 photoisomer in mammalian cells ($t_{1/2} \approx 5.5$ min)[5].

[1]Department of Bioengineering, University of California, Berkeley (UC Berkeley), Berkeley, California, USA. [2]The UC Berkeley–UCSF Graduate Program in Bioengineering, UC Berkeley, Berkeley, California, USA. [3]Department of Chemical Engineering, UC Berkeley, Berkeley, California, USA. [4]Howard P. Isermann Department of Chemical and Biological Engineering, Rensselaer Polytechnic Institute, Troy, New York, USA. [5]Center for Biotechnology and Interdisciplinary Studies, Rensselaer Polytechnic Institute, Troy, New York, USA. [6]Helen Wills Neuroscience Institute, UC Berkeley, Berkeley, California, USA. [7]California Institute for Quantitative Biosciences, UC Berkeley, Berkeley, California, USA. Correspondence should be addressed to R.S.K. (kaner@rpi.edu) or D.V.S. (schaffer@berkeley.edu).

RECEIVED 3 JULY 2012; ACCEPTED 3 JANUARY 2013; PUBLISHED ONLINE 3 FEBRUARY 2013; DOI:10.1038/NMETH.2360

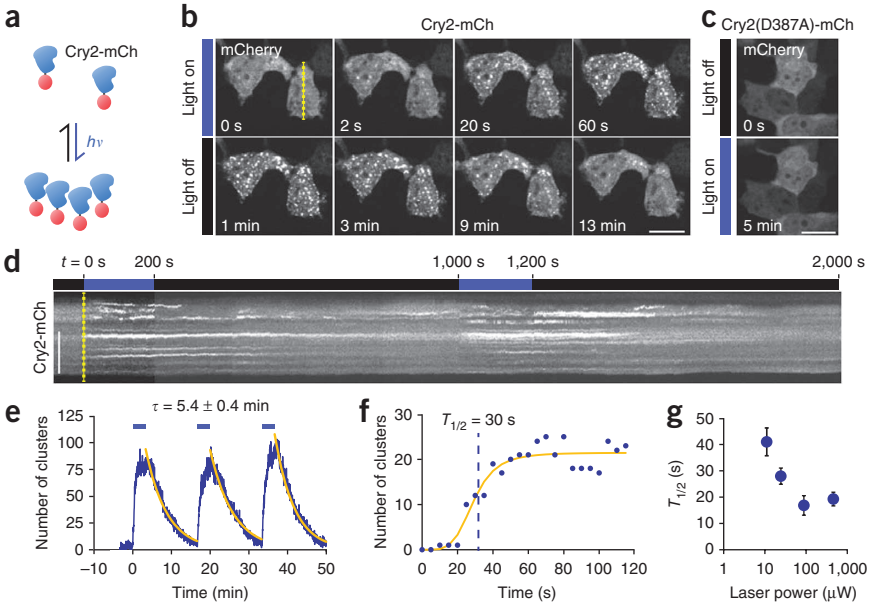

Figure 1 | Cry2-mCh oligomerizes under blue light in mammalian cells. (**a**) Schematic depicting light-induced protein clustering. *hν*, light activation energy as given by the Planck relation. (**b**) Cry2-mCh cluster formation (top) in HEK 293T cells in response to 488-nm laser light, as well as dissociation (bottom) after light withdrawal. Scale bars (**b**–**d**), 20 μm. (**c**) Clustering does not occur with the light-insensitive mutant Cry2(D387A)-mCh. (**d**) Kymograph of mCherry fluorescence corresponding to the dashed line in **b**. (**e**) Measurement of cluster number over multiple light-dark cycles demonstrates repeatable, rapid clustering and declustering with consistent kinetics. A single exponential decay fit of cluster number allows measurement of cluster decay constant τ (mean ± 1 s.d., n = 3 decay cycles). (**f**) Representative plot of single-cell cluster formation over time. Similar behavior was observed in all cells for which cluster formation was measured. $T_{1/2}$, time at which a half-maximal number of visible clusters was detected. (**g**) Representative plot of concentration-normalized $T_{1/2}$ increase with decreased illuminating intensity (Online Methods). Plot shows mean ± 1 s.e.m., n = 4 cells for each condition.

We next investigated whether inducible Cry2-mCh clustering could be harnessed to induce oligomerization-dependent signaling. Canonical Wnt/β-catenin signaling is triggered by Wnt ligand binding to Frizzled and LRP6 co-receptors, which then form higher-order clusters[14] and activate β-catenin. Upon activation, β-catenin translocates to the nucleus and functions as a transcriptional cofactor to activate key targets. Recently, constitutive clustering of just the LRP6 C-terminal domain (LRP6c) was shown to robustly activate β-catenin signaling[15]. By adding either one or three chemically induced dimerizing domains, we found that LRP6c oligomerization is indeed necessary—and dimerization is insufficient—to activate β-catenin signaling (**Supplementary Fig. 4**).

To determine whether the LRP6c endodomain could be oligomerized in response to light, and thus offer spatiotemporally precise control over canonical Wnt signaling (**Fig. 2a**), we fused it to the C terminus of Cry2-mCh (Cry2-LRP6c). In HEK 293T cells expressing this fusion, visible puncta appeared within 2 s of blue light exposure, and these clusters dissociated upon light withdrawal with somewhat slower kinetics than those observed with Cry2-mCh (**Fig. 2b** and **Supplementary Video 3**). To assess whether this clustering could induce pathway activation, we transfected cells carrying a β-catenin–responsive luciferase reporter[16] with Cry2-LRP6c. Blue light illumination led to elevated levels of active β-catenin, accompanied by considerably higher levels of luciferase activity, in Cry2-LRP6c cells relative to unilluminated

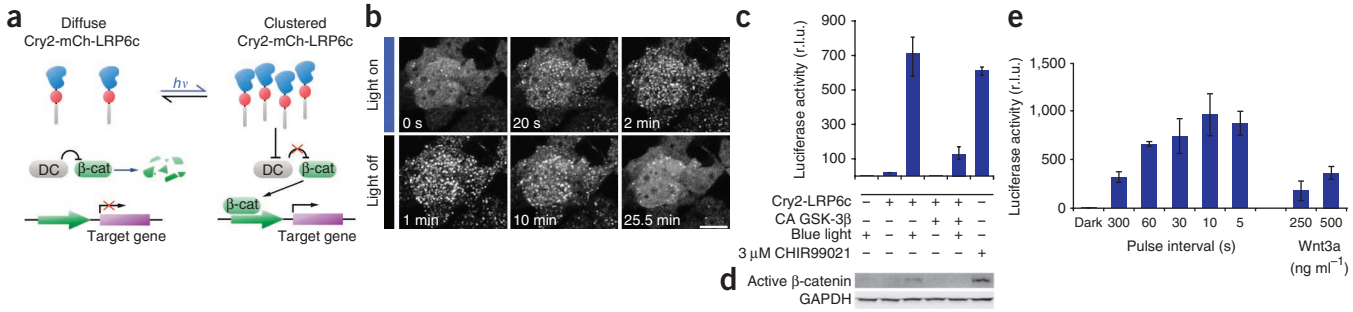

Figure 2 | Light-induced Cry2-LRP6c clustering modulates the Wnt/β-catenin pathway. (**a**) Schematic of photoactivation strategy. Upon light (*hν*) activation, clustering of the LRP6c domain inhibits the destruction complex (DC), relieving β-catenin (β-cat) inhibition and allowing its translocation to the nucleus and regulation of target-gene transcription. (**b**) Cry2-LRP6c retains the ability to reversibly cluster in HEK 293T cells. Scale bar, 20 μm. (**c**) Light-induced β-catenin transcriptional activity assayed in HEK 293T cells carrying Cry2-LRP6c and a luciferase reporter shows strong β-catenin activity after 16-h exposure to blue light pulses (500-ms pulse every 10 s). The light-induced signal was attenuated in the presence of constitutively active (CA) β-catenin pathway inhibitor GSK-3β and was comparable to that observed with small-molecule pathway agonist CHIR99021 (3 μM). Graph shows mean ± 1 s.d., n = 3 replicates. (**d**) Western blot for active β-catenin levels in HEK 293T cells under conditions as in **c**. (**e**) Neural stem cells carrying the luciferase reporter and expressing Cry2-LRP6c strongly upregulated luciferase in response to Wnt3a protein or to 500-ms light pulses for 16 h, with the interval between pulses varying from 5–300 s. Graph is representative of three independent experiments, and error bars show the range of duplicate samples. r.l.u., relative light units.

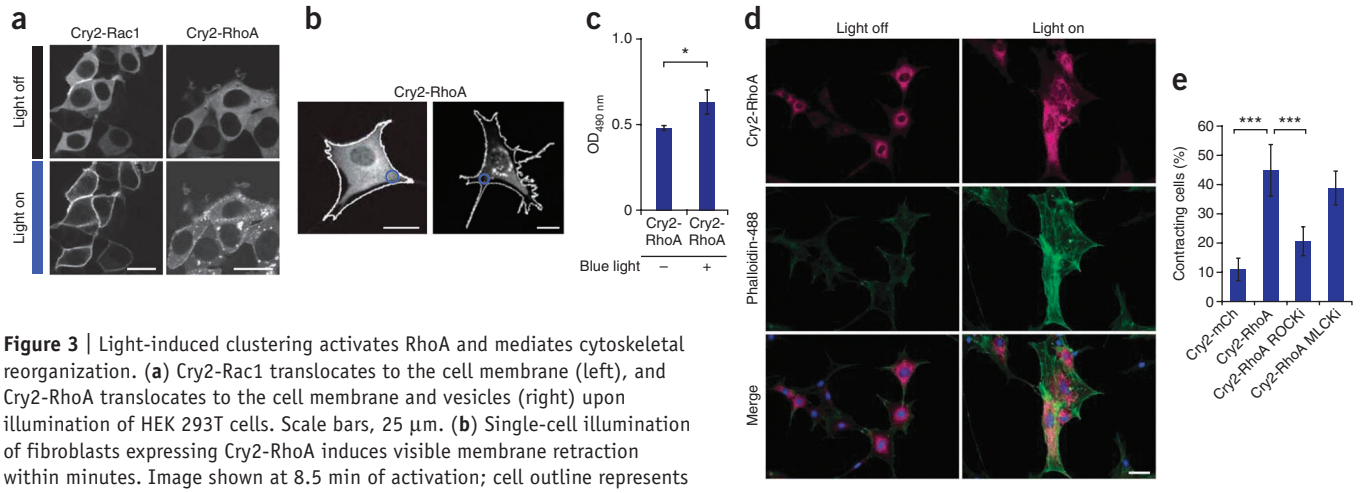

Figure 3 | Light-induced clustering activates RhoA and mediates cytoskeletal reorganization. (**a**) Cry2-Rac1 translocates to the cell membrane (left), and Cry2-RhoA translocates to the cell membrane and vesicles (right) upon illumination of HEK 293T cells. Scale bars, 25 µm. (**b**) Single-cell illumination of fibroblasts expressing Cry2-RhoA induces visible membrane retraction within minutes. Image shown at 8.5 min of activation; cell outline represents starting cell morphology, and circles depict illumination region. Scale bars, 20 µm. (**c**) ELISA analysis shows that cells expressing Cry2-RhoA have increased levels of GTP-bound (active) RhoA under blue light as compared to unilluminated controls (mean ± 1 s.d., $n = 3$ replicates, $^*P = 0.0495$). OD, optical density. (**d**) Cry2-RhoA photoactivation induces enhanced stress-fiber formation in fibroblasts as visualized by the actin-binding Alexa Fluor 488–phalloidin conjugate. Scale bar, 50 µm. (**e**) Whole-field light activation induces contractility in fibroblasts expressing Cry2-RhoA. Inhibition with Rho-associated kinase inhibitor Y-27632 (ROCKi), but not myosin light chain kinase inhibitor ML-7 (MLCKi), attenuates this effect, thus demonstrating dependence of light-induced membrane retraction on RhoA pathway activation and independence from MLCK activity. Graph shows means ± 1 s.d., $n = 6$–10 fields, $^{***}P < 0.001$.

or untransfected controls (**Fig. 2c**,**d**). Coexpression of constitutively active GSK-3β, a β-catenin signaling antagonist, attenuated the β-catenin and luciferase signals, thus indicating specificity of pathway activation. Furthermore, the light-induced Cry2-LRP6c transcriptional response was similar to that observed using the strong pathway agonist CHIR99021, which suggests a large dynamic range of activation (**Fig. 2c**,**d**). Despite the similar transcriptional response, these two conditions exhibited differentially elevated levels of active β-catenin (**Fig. 2d**), potentially because of a nonlinear or dynamic relationship between active β-catenin levels and induced luciferase expression or activity.

To generalize these results to another cell type and to determine whether low construct copy numbers could yield similar results, we introduced Cry2-LRP6c via a retroviral vector into neural stem cells harboring the β-catenin luciferase reporter. Upon illumination with a custom-built device that allows control of pulse width and frequency (**Supplementary Fig. 5**), cells demonstrated a strong dose responsiveness to increased blue light pulse frequency ($P = 0.0051$, $n = 2$ replicates, Jonckheere-Terpstra trend analysis, **Fig. 2e**), whereas cells kept in the dark yielded a negligible readout. Maximal light-induced signaling increased luciferase expression ~200-fold over that of unilluminated controls and greatly exceeded reporter expression induced by high levels of pathway agonist Wnt3a (**Fig. 2e**), further demonstrating tunability of β-catenin activity over a large signaling range. The ability to dynamically control β-catenin activity may lead to insights throughout the numerous biological systems in which this molecule plays a central role.

We next investigated the modularity of Cry2-mCh as a general tool for clustering proteins and activating other signaling pathways. Rho GTPases are small proteins involved in actin polymerization, cell motility and mechanotransduction[17]. Oligomerization of the Rho GTPase Rac1 has been reported to enhance its enzymatic activity and effector activation in *in vitro* assays[18], though the functional significance of Rac1 oligomerization in living cells has not, to our knowledge, been studied. Within 2 s of illumination, HEK 293T cells expressing a fusion of Cry2-mCherry with Rac1 (Cry2-Rac1) demonstrated translocation of mCherry fluorescence from the cytoplasm to the membrane, a hallmark of Rho GTPase activation, accompanied by apparent cell spreading, suggesting Rac1 activation[19] (**Fig. 3a**, **Supplementary Fig. 6** and **Supplementary Video 4**).

Because a different strategy was recently used to generate a photoactivatable Rac1 (ref. 20), we applied our inducible clustering approach to a distinct Rho GTPase family member. RhoA is a small GTPase primarily responsible for mediating cellular tension and cytoskeletal contraction. Photocontrol of RhoA has not yet been achieved, and oligomerization has not been linked to RhoA activity. Notably, when we added a constitutively oligomerizing DIX domain to mCherry-RhoA, the resulting protein was membrane localized (**Supplementary Fig. 7**). Similarly, a Cry2-mCherry-RhoA fusion (Cry2-RhoA) was initially diffuse but translocated to membranes and vesicles within seconds of activation with 458-nm or 488-nm laser light (10 µW) in HEK 293T cells (**Fig. 3a**, **Supplementary Fig. 6** and **Supplementary Video 5**) and NIH 3T3 fibroblasts (**Supplementary Fig. 8**). This translocation did not occur in cells expressing RhoA and Cry2 on separate peptide chains (**Supplementary Video 6**), which suggests it was not due to nonspecific effects of Cry2 photoisomerization. Furthermore, within minutes of single-cell illumination, cellular membrane retraction was evident (**Fig. 3b** and **Supplementary Videos 7** and **8**), suggesting that the RhoA translocation coincided with RhoA activation. Finally, both membrane retraction and Cry2-RhoA membrane localization were reversible within minutes, and cells could be repeatedly activated and inactivated (**Supplementary Video 9**).

To verify that Cry2-mediated clustering was inducing RhoA activation, we used an ELISA assay (**Fig. 3c**) to probe for changes in levels of activated (GTP-bound) RhoA protein upon illumination of fibroblasts expressing Cry2-RhoA. Light exposure induced

a significant increase in RhoA-GTP levels compared to those of unilluminated controls ($P = 0.0495$, Mann-Whitney-Wilcoxon test, $n = 3$ replicates, representative of five experiments), though the level of biochemical activation may have been lower than expected from the observed phenotype owing to the presence of a majority fraction of native (uninducible) RhoA in the cells (**Supplementary Fig. 9**).

To further characterize activity, we examined the induction of stress fibers, bundles of filamentous actin that form in response to RhoA activation and mediate cytoskeletal contraction[21]. Illuminated fibroblasts expressing Cry2-RhoA showed a strong increase in both the number and intensity of stress fibers as compared to unilluminated controls (**Fig. 3d**). Notably, in highly expressing cells, light-induced Cry2-RhoA clusters visibly orient along—and in many cases colocalize with—the stress fibers.

We tested the functional specificity of the photoclustered RhoA response by observing fibroblast cell-membrane retraction in the presence of pathway inhibitors (**Supplementary Video 10**). Illuminated cells expressing Cry2-RhoA contracted at a higher frequency than cells expressing Cry2-mCh ($P < 0.001$, Tukey-Kramer test, $n = 6$ and 8 fields of view, **Fig. 3e**). Furthermore, inhibition of the RhoA downstream effector Rho-associated protein kinase (ROCK) with the small molecule Y-27632 reduced the percentage of contractile cells ($P < 0.001$, Tukey-Kramer test, $n = 8$ and 8), but inhibition of myosin light chain kinase, which mediates contraction independently of RhoA and ROCK, did not ($P = 0.3$, Tukey-Kramer test, $n = 8$ and 10 control and inhibited trials, respectively), indicating that the light-induced contractile response is in large part specific to RhoA activity. Taken together, these data strongly suggest that Cry2-mediated light-inducible clustering of RhoA activates the RhoA pathway and induces cytoskeletal remodeling.

Cry2-mediated protein clustering can modulate diverse signaling pathway activities in a dynamic manner, offering an approach to quantitatively investigate signal transduction dynamics and to analyze oligomerization as a potentially important mechanism in cellular signaling. The modular, genetically encodable and single-construct nature of Cry2, which can be adapted to additional signal transducers in the future, thus provides a versatile protein clustering system with potential to extend the benefits of precise photoactivation to numerous signaling molecules and pathways.

METHODS

Methods and any associated references are available in the online version of the paper.

Note: Supplementary information is available in the online version of the paper.

ACKNOWLEDGMENTS

We thank S. Kumar for technical discussions and use of equipment and reagents, and J. McKay and S. Rammensee for experimental advice and assistance. We received the *CRY2PHR-mCherry* construct as a gift from C. Tucker (Duke University), constitutively active variants of Rac1, RhoA and Cdc42 as gifts from G.S. Martin (UC Berkeley), the full-length *LRP6* construct as a gift from X. He (Harvard University) and CA-β-catenin as a gift from A. Asthagiri (Northeastern University). We would also like to thank M. Niewiadomska-Bugaj (Western Michigan University) for statistical analysis, A. Keung (UC Berkeley) for retroviral constructs encoding the Rho GTPases and A. Fritz (UC Berkeley) for retroviral constructs encoding CA-β-catenin and CA-GSK-3β. This work was supported by the US Department of Energy, Office of Basic Energy Sciences, Division of Materials Sciences and Engineering, under Award nos. DE-SC0001216 and DE-SC0001874.

AUTHOR CONTRIBUTIONS

D.V.S., R.S.K. and L.J.B. conceived the idea. D.V.S. and L.J.B. directed the work. L.J.B., A.T.C. and C.K.M. performed experiments. L.J.B. wrote the manuscript with revision and editing from D.V.S. and R.S.K.

COMPETING FINANCIAL INTERESTS

The authors declare no competing financial interests.

Published online at http://www.nature.com/doifinder/10.1038/nmeth.2360/. Reprints and permissions information is available online at http://www.nature.com/reprints/index.html.

1. Dehmelt, L. & Bastiaens, P.I.H. *Nat. Rev. Mol. Cell Biol.* **11**, 440–452 (2010).
2. Mammen, M., Choi, S.-K. & Whitesides, G.M. *Angew. Chem. Int. Edn Engl.* **37**, 2754–2794 (1998).
3. Spencer, D.M., Wandless, T.J., Schreiber, S.L. & Crabtree, G.R. *Science* **262**, 1019–1024 (1993).
4. Möglich, A. & Moffat, K. *Photochem. Photobiol. Sci.* **9**, 1286–1300 (2010).
5. Kennedy, M.J. *et al. Nat. Methods* **7**, 973–975 (2010).
6. Levskaya, A., Weiner, O.D., Lim, W.A. & Voigt, C.A. *Nature* **461**, 997–1001 (2009).
7. Strickland, D. *et al. Nat. Methods* **9**, 379–384 (2012).
8. Yazawa, M., Sadaghiani, A.M., Hsueh, B. & Dolmetsch, R.E. *Nat. Biotechnol.* **27**, 941–945 (2009).
9. Shimizu-Sato, S., Huq, E., Tepperman, J.M. & Quail, P.H. *Nat. Biotechnol.* **20**, 1041–1044 (2002).
10. Wang, X., Chen, X. & Yang, Y. *Nat. Methods* **9**, 266–269 (2012).
11. Más, P., Devlin, P.F., Panda, S. & Kay, S.A. *Nature* **408**, 207–211 (2000).
12. Liu, H. *et al. Science* **322**, 1535–1539 (2008).
13. Hollander, M. & Wolfe, D.A. *Nonparametric Statistical Methods* 2nd edn. (Wiley, New York, 1999).
14. Bilić, J. *et al. Science* **316**, 1619–1622 (2007).
15. Metcalfe, C., Mendoza-Topaz, C., Mieszczanek, J. & Bienz, M. *J. Cell Sci.* **123**, 1588–1599 (2010).
16. Fuerer, C. & Nusse, R. *PLoS ONE* **5**, e9370 (2010).
17. Jaffe, A.B. & Hall, A. *Annu. Rev. Cell Dev. Biol.* **21**, 247–269 (2005).
18. Zhang, B., Gao, Y., Moon, S.Y., Zhang, Y. & Zheng, Y. *J. Biol. Chem.* **276**, 8958–8967 (2001).
19. Parsons, J.T., Horwitz, A.R. & Schwartz, M.A. *Nat. Rev. Mol. Cell Biol.* **11**, 633–643 (2010).
20. Wu, Y.I. *et al. Nature* **461**, 104–108 (2009).
21. Ridley, A.J. & Hall, A. *Cell* **70**, 389–399 (1992).

ONLINE METHODS

Cloning and viral production. The *LRP6* C terminus[15] was amplified from pCS2+ *LRP6* and inserted into the *CRY2PHR-mCherry* plasmid between BsrGI and XbaI sites, which resulted in *CRY2-mCherry*-linker-*LRP6c*, with the linker GGGGSGGGGS. We created 1× and 3× *DmrB-mCh-LRP6c* constructs by first amplifying the DmrB domain from pMSCV-F-del-Casp9.IRES.GFP (Addgene: 15567) and inserting upstream of *mCh-LRP6c* through the CPEC method[22]. *RAC1* and *RHOA* were subcloned into *CRY2PHR-mCherry* between BsrGI and NotI with the same linker as for *LRP6c*. *CRY2* fusions were then subcloned into the MMLV retroviral vector CLPIT or CLGPIT, which provide tetracycline-repressible transgene control. The virus was packaged as described[23], in the presence of 100 ng/mL doxycycline to repress transgene expression. CA-*GSK3B* was generated by point mutagenesis of sequence recovered from neural stem cell (NSC) cDNA via RT-PCR and was cloned into CLPIT. A lentiviral plasmid encoding the 7× TFP luciferase reporter was obtained from Addgene (24308) and was packaged in HEK 293T cells. Stable cell lines were created through infection and puromycin selection.

A detailed list of constructs appears in **Supplementary Table 1**. *LRP6c*, *RAC1* and *RHOA* fusions will be made available through Addgene (http://www.addgene.org/).

Cell culture. HEK 293T cells were cultured on polystyrene plates in Iscove's Modified Dulbecco's Medium (Corning Cellgro) with 10% FBS (FBS) (Life Technologies) and 1% penicillin/streptomycin (P/S) (Life Technologies) at 37 °C and 5% CO_2. Rat hippocampal adult NSCs[24] were cultured on polystyrene plates coated with polyornithine and 5 μg/mL laminin (Life Technologies). NSCs were cultured in Dulbecco's Modified Eagle Medium (DMEM)/F12 (1:1) high-glucose medium containing N-2 supplement (both from Life Technologies) and 20 ng/mL recombinant human FGF-2 (PeproTech). Illumination experiments were conducted in the presence of 0.5% FBS, which was used to provide carrier protein for Wnt3a (R&D Systems). NIH 3T3 fibroblasts were cultured in DMEM (Corning Cellgro) supplemented with 10% bovine calf serum (BCS) and 1% P/S. Stable cell lines expressing the *Cry2-RhoA* construct were maintained in 100 ng/mL tetracycline to repress expression, as high levels of sustained Cry2-RhoA expression impaired cell growth. Tetracycline was withdrawn 24 h before contractility experiments and replaced with 1 ng/mL doxycycline, and serum was reduced to 2%.

Luciferase assay. For chemically induced oligomerization experiments, 293T cells harboring the 7× TCF luciferase reporter were seeded in 48-well plates. When they were ~70% confluent, cells were transfected with 300 ng of the expression vectors and 150 ng pBluescript by the calcium phosphate method. 24 h after transfection, 500 nM of B/B Homodimerizer (Clontech) was added to designated wells. After 16 h of treatment, cells were lysed, and luciferase was measured with the Luc-screen Firefly Luciferase Gene Reporter System (Life Technologies). Experiments testing Cry2-LRP6c function were carried out in a similar manner, but cells were seeded in black-walled 96-well plates, and only 5 ng of expression vector diluted in 150 ng pBluescript were transfected. Twenty-four hours after transfection, cells were subjected to a light illumination protocol from a custom LED illumination device. Briefly, an LED array was constructed based on the open-source electronics Arduino platform (http://www.arduino.cc/). 5-mm blue LEDs (470 nm, 6,000 millicandelas, 20° illumination, http://www.electron.com/) with a 3-mW measured output (Coherent) were placed underneath wells of a 96-well plate and were driven through independent channels by the Arduino. The device is pictured in **Supplementary Figure 5**. The plate with cells was placed on top of the LED device so that the LEDs illuminated directly underneath individual wells. 500-ms blue light pulses were administered every 10 s. After 16 h of illumination, cells were lysed, and luciferase was measured as above. For NSC experiments, cells carrying the 7× TCF reporter were seeded in a 35-mm dish and infected with retrovirus encoding Cry2-LRP6c at a multiplicity of infection of 3. After 2 d, cells were seeded at 80,000 cells per well in a black-walled, 96-well, laminin-coated plate, and after 1 h cells were illuminated with the custom LED array for 16 h. Luciferase readout from NSCs was measured as above.

Immunoblotting. Cells were lysed with RIPA buffer containing protease inhibitors, and cell lysates were electrophoretically separated on an SDS-PAGE gel. Proteins were then transferred onto a nitrocellulose membrane and probed for active β-catenin (Millipore, clone 8E7, cat. #05-665, 1:500 dilution) and RhoA (Cell Signaling, cat. 2117, 1:1,000 dilution) and with GAPDH (Abcam, cat. #ab9485, 1:2,500 dilution) as a loading control.

Stress-fiber visualization. We serum-starved Cry2-RhoA–expressing NIH 3T3s by seeding at 2,500 cells per cm^2 on glass-bottom six-well plates (MatTek Corporation) in DMEM/F12 (Life Technologies) supplemented with 1% P/S, 10% FBS, and 100 ng/mL tetracycline. After 24 h, cells were gently washed twice with PBS, and the same medium was added but with 0.1% FBS. 24 h later, the process was repeated, but serum-free medium was added and tetracycline withdrawn. Cells were repeatedly pulsed (3 s on, 12 s off) with light from a blue 19-LED array (http://ledlight.com/, cat. #28345) for 10 min and then immediately fixed in 4% paraformaldehyde. Cells were incubated in Alexa 488–conjugated phalloidin (Life Technologies) and DAPI diluted in phosphate buffered saline containing 0.3% Triton X-100 for 30 min. Images were obtained through epifluorescence microscopy using a TE2000-E2 microscope (Nikon).

ELISA. Cry2-RhoA–expressing NIH 3T3 cells were seeded in six-well plates at 70,000 cells per well and were serum-starved over 3 d, as above. After 24 h in serum-free medium supplemented with 1 ng/mL doxycycline, cells were exposed to 2 min of blue LED light. The samples were processed, and the levels of GTP-loaded (active) RhoA were determined using the G-LISA RhoA Activation Assay Biochem Kit (Cytoskeleton) according to manufacturer instructions. This ELISA-based assay uses the differential binding of GDP- vs. GTP-loaded RhoA to the binding domain of rhotekin to determine the relative levels of only active RhoA in a sample.

Live-cell imaging. Time-lapse microscopy of activated Cry2 fusions in HEK 293T cells was performed using a BX51WI

microscope (Olympus) equipped with swept-field confocal technology (Prairie Technologies). Clustering visualization in 293T cells was carried out at room temperature. Simultaneous blue light exposure and mCherry imaging was accomplished by imaging in both 488-nm and 561-nm laser channels, one exposure per 2–5 s, with the 488-nm laser varied between 0.1% and 100% power. Given the minutes-long timescale of the dissociation kinetics of Cry2 clustering, this intermittent pulsing was considered a sufficient approximation of continuous exposure and was necessary to avoid extensive photobleaching of the mCherry fluorophore. Focal illumination of NIH 3T3 cells expressing Cry2-RhoA was performed on a Zeiss LSM 710 AxioObserver confocal microscope with full incubation chamber in conjunction with the Zeiss ZEN software. All experiments were carried out at 37 °C and in 5% CO_2. mCherry was visualized with 561-nm laser excitation through a 63× oil-immersion objective, and blue light focal illumination was carried out through the FRAP application with the 458-nm laser light between 0.1%–10% power for 6–100 µs dwell time per pixel in a 10-µm-diameter region. FRAP, *z* stacks, and time-lapse microscopy observing cluster formation were also acquired with the Zeiss LSM 710. For wide-field contractility measurements, cells were imaged under bright field using a Nikon Eclipse Ti inverted microscope and exposed to 200-µs pulses of blue light from a xenon arc lamp passed through a GFP filter cube. Pulses were delivered every 20 s for 10 min, and images were assembled in ImageJ. Contraction was determined by membrane retraction, which was assessed through visual inspection, and the number of contracting cells was divided by total number of cells in the field to obtain the percentage of contracting cells.

Image analysis. Stacks of single-cell clustering time-lapse images were assembled in ImageJ (http://rsbweb.nih.gov/ij/). Clusters were then counted in each frame of the time lapse in CellProfiler (http://www.cellprofiler.com/) by first thresholding the fluorescence image so that the software recognized clusters in the right intensity range. This appropriate threshold was determined manually for each cell because of cell-to-cell fluorescence intensity variation. Plotting cluster number vs. time yielded a sigmoidal relationship, which was fit to the Hill function for the purposes of extracting $T_{1/2}$, the time at which the cluster number reached half of its final value

$$C = \frac{t^n}{t^n + T_{1/2}^n}$$

where C represents cluster number, t is time and n is the Hill coefficient. $T_{1/2}$ provides a metric by which to compare clustering conditions. To demonstrate the dependence of clustering on laser power, we plotted $T_{1/2}$ vs. 488-nm laser power after normalization by mean cell fluorescence to correct for protein expression level differences. To determine the relationship between mean cell fluorescence and $T_{1/2}$, we measured $T_{1/2}$ for cells at four different laser intensities, and for each laser intensity setting, linear relationships were observed between mean cell fluorescence and $T_{1/2}$. The means of the slopes of the linear fit for each laser setting were averaged, and this value represented the estimated change in $T_{1/2}$ per change in mean cell fluorescence. Individual $T_{1/2}$ values were then adjusted by this factor to effectively normalize protein concentration among all cells.

Quantitation of fluorescence relocalization in HEK 293T cells expressing Cry2-Rac1 and Cry2-RhoA was accomplished by the following algorithm:

$$\frac{I_{\mathrm{Cyto},t} - I_{\mathrm{Nuclear},t}}{I_{\mathrm{Cyto,initial}} - I_{\mathrm{Nuclear,initial}}}$$

where $I_{\mathrm{Cyto},t}$ and $I_{\mathrm{Nuclear},t}$ are cytoplasmic and nuclear fluorescence intensity at time t, respectively, and $I_{\mathrm{Cyto,initial}}$ and $I_{\mathrm{Nuclear,initial}}$ are the initial values of cytoplasmic and nuclear fluorescence.

Statistical analysis. All statistical analysis was performed using the JMP v.10 software. Jonckheere-Terpstra trend analysis is a nonparametric method used to ascertain whether population medians have an a priori ordering. The Mann-Whitney-Wilcoxon test is a nonparametric method for comparing two sample sets. For details on both, see ref. 13.

22. Quan, J. & Tian, J. *PLoS ONE* **4**, e6441 (2009).
23. Peltier, J. & Schaffer, D.V. in *Protocols for Adult Stem Cells* Vol. 621 (eds. Conboy, I.M., Schaffer, D.V., Barcellos-Hoff, M.H. & Li, S.) Ch. 7, 103–116 (Humana, 2010).
24. Gage, F.H. *et al. Proc. Natl. Acad. Sci. USA* **92**, 11879–11883 (1995).

doi:10.1038/nmeth.2360